



# Preparation and Performance of a $\text{La}_{0.6}\text{Sr}_{0.4}\text{Co}_x\text{Fe}_{1-x}\text{O}_3$ Cathode for Solid Oxide Fuel Cells

Pan Wang<sup>1</sup> · Jihai Cheng<sup>1</sup>

Received: 28 February 2022 / Accepted: 10 August 2022 / Published online: 30 August 2022  
© The Minerals, Metals & Materials Society 2022

## Abstract

In this study, a potential cathode material,  $\text{La}_{0.6}\text{Sr}_{0.4}\text{Co}_x\text{Fe}_{1-x}\text{O}_3$  (LSCF), for intermediate-temperature solid oxide fuel cells (SOFCs) is synthesized via a citric acid-assisted combustion method. The electrolyte-supported solid oxide fuel cell is formed in a conventional way to estimate the cell performance. Results show that the as-prepared powders have a pure perovskite structure after calcination at 1050°C, and the initial powders have a fluffy and spongy mass with a porous structure. The cell performance is affected by the LSCF powder morphology and calcination temperature. The peak power density of the  $\text{Y}_2\text{O}_3$ -stabilized  $\text{ZrO}_2$  (YSZ) electrolyte-supported single cell using LSCF as cathode is  $28 \text{ mW cm}^{-2}$  at 800°C, while the smallest area-specific resistance obtained is  $19 \Omega \text{ cm}^2$ . This suggests that  $\text{La}_{0.6}\text{Sr}_{0.4}\text{Co}_x\text{Fe}_{1-x}\text{O}_3$  is a promising potential cathode material for SOFCs.

**Keywords** Solid oxide fuel cell · cathode · electrochemical performance · area-specific resistance

## Introduction

With the rapid pace of economic development and social progress, the use of fossil fuels has increased dramatically. Excessive use of fossil fuels not only causes the depletion of resources, but also causes great pollution of the environment.<sup>1</sup> As the demand for clean energy increases, sustainable energy and new energy conversion facilities are gaining traction.<sup>2</sup> A fuel cell is a device that converts chemical energy directly into electrical energy.<sup>3</sup> Compared with other fuel cells, solid oxide fuel cells (SOFCs) have the advantages of low cost, low pollution, high utilization rate and high conversion rate, and have great development potential.<sup>4,5</sup> However, traditional SOFCs based on  $\text{Y}_2\text{O}_3$ -stabilized  $\text{ZrO}_2$  (YSZ) electrolytes must work at high temperatures, and there are some technical and economical obstacles for SOFCs working at high temperatures for long periods.<sup>6</sup> Thus, intermediate-temperature SOFCs operating below 800°C have attracted much attention, as this operation enables the use of low-cost metal interconnects, provides long-term cell

material stability, and reduces the material corrosion of factory components.<sup>7,8</sup>

Several composite oxides with a perovskite structure have been used as cathode materials for intermediate-temperature SOFCs (600–800°C),<sup>9</sup> because of their high electric and ionic conductivity and high catalytic activity for oxygen.<sup>10–13</sup> Among these materials, compounds containing La and Sr on the A-site and Co and/or Fe on the B-site have been widely studied for SOFCs.<sup>14,15</sup> The results indicate that the sintering temperature influences the conductivity, microstructure and electrochemical performance. Giuseppe et al. investigated the effect of different sintering temperatures on the electrochemical properties of  $\text{La}_{0.6}\text{Sr}_{0.4}\text{Co}_x\text{Fe}_{1-x}\text{O}_3$  (LSCF) cathode materials and found that the cell performance increased with the increase in sintering temperature.<sup>16</sup> Zhou et al. studied the effect of cerium doping for the performance of LSCF cathodes.<sup>17</sup> The electrochemical performance of LSCF was enhanced with the increase in cerium content.

The aim of this work is to investigate the effect of introducing cobalt into strontium lanthanum ferrite on the structure of the material. With respect to its use as SOFC cathode, the effect of the presence of cobalt on the electrochemical performance is investigated in detail. Therefore, the present work is focused on determining the effects of cobalt content and calcination temperature on the performance of electrolyte-supported SOFCs using LSCF as cathode materials.

✉ Jihai Cheng  
hdcheng256@hotmail.com

<sup>1</sup> School of Energy Materials and Chemical Engineering, Hefei University, Hefei 230601, China

We attempt to substitute  $\text{Fe}^{3+}$  in  $\text{La}_{0.6}\text{Sr}_{0.4}\text{FeO}_3$  with  $\text{Co}^{3+}$ . In addition, we elucidate the relationship between the Co-substituted  $\text{La}_{0.6}\text{Sr}_{0.4}\text{FeO}_3$  crystal structure and its electrochemical performance, with the aim of developing novel cathode materials that can be used in low- and intermediate-temperature SOFCs.

## Experimental

### Preparation of LSCF Powders

The  $\text{La}_{0.6}\text{Sr}_{0.4}\text{Co}_x\text{Fe}_{1-x}\text{O}_3$  ( $x=0.2, 0.4, 0.6$ ) powders were prepared via a citric acid-assisted combustion method. In the process,  $\text{Fe}(\text{NO}_3)_3 \cdot 6\text{H}_2\text{O}$ ,  $\text{Sr}(\text{NO}_3)_2 \cdot 6\text{H}_2\text{O}$ ,  $\text{Co}(\text{NO}_3)_2 \cdot 6\text{H}_2\text{O}$  and  $\text{La}(\text{NO}_3)_3 \cdot 6\text{H}_2\text{O}$  were used as the raw materials. All raw materials were analytically pure and purchased from China Sinopharm Chemical Reagent Co., Ltd.

The four nitrates were dissolved in deionized water and mixed together. Citric acid was also dissolved in deionized water, and the citric acid solution was then slowly added to the aqueous solution of the metallic salts under constant stirring. The molar ratio of citric acid to metal ions (Ce, Sm, Fe) was 1.5:1. The complexation process of citric acid increases the solubility of metal ions and helps to maintain homogeneity by preventing their selective precipitation. The precursor solution was stirred at  $80^\circ\text{C}$  and then converted to a viscous gel. The gel was subsequently heated until it ignited, and then formed metal-oxide “ash.” The collected “ash” was sintered at different temperatures for 2 h to form  $\text{La}_{0.6}\text{Sr}_{0.4}\text{Co}_x\text{Fe}_{1-x}\text{O}_3$  powders.

### Assembly of the Fuel Cell

In order to assemble a single cell, we selected YSZ as the electrolyte. YSZ powders with purity of 99.99% were purchased from Jiangsu Lida High-Tech Special Materials Co., Ltd., China. Commercially available YSZ powders with size of  $1.0\ \mu\text{m}$  were pressed into discs under 200 MPa and then calcined in air at  $1400^\circ\text{C}$  for 5 h to obtain electrolyte discs (about  $300\ \mu\text{m}$  in thickness) with relative density over 95%. The density of the sintered body is determined by the standard Archimedes method.

NiO and YSZ powders with a mass ratio of 1.5:1 were mixed together and ground in an agate mortar for 1 h, after which a certain amount of terpineol was added and ground for 2 h to form an anode slurry. The mass ratio of solids to terpineol was 75:25. The slurry was screen-printed on one side of the YSZ electrolyte disc and then calcined at  $1350^\circ\text{C}$  for 2 h. With a similar method, a cathode slurry consisting of the as-prepared

$\text{La}_{0.6}\text{Sr}_{0.4}\text{Co}_x\text{Fe}_{1-x}\text{O}_3$  powders and terpineol was screen-printed onto the other side of the electrolyte disc and calcined at  $1200^\circ\text{C}$  for 1 h. The electrodes have an effective area of  $1.0\ \text{cm}^2$  with a thickness of about  $50\ \mu\text{m}$ . Thus, a single cell with the structure Ni-YSZ|YSZ|LSCF was assembled.

### Characterization

The crystal structure of  $\text{La}_{0.6}\text{Sr}_{0.4}\text{Co}_x\text{Fe}_{1-x}\text{O}_3$  powders were characterized by x-ray diffraction (XRD, Rigaku SmartLab 9 kW diffractometer, Japan). The diffractograms were scanned in  $2\theta$  from  $10^\circ$  to  $80^\circ$  using  $\text{Cu K}\alpha$  line ( $\lambda=0.154056\ \text{nm}$ ) with a scan step size of 0.05 and single point time of 0.5 s. The obtained data were processed using Jade software. The microstructure of LSCF samples were examined by scanning electron microscopy (SEM, Hitachi SU8010, Japan) at accelerating voltage of 5 and 15 kV. For electrochemical measurement, the cell was sealed in an alumina tube with a silver paste. The silver paste was coated on each electrode as current collector. During the test, the cell was slowly heated from room temperature to the desired temperature, and the NiO was reduced to Ni by hydrogen until the open-circuit voltage of the cell was stable.<sup>18</sup> Electrochemical impedance spectroscopy (EIS) measurements were taken using an electrochemical analyzer (CHI604C, Chenhua, China). Measurement of the data was conducted over a frequency range of 0.1 Hz to 100 kHz from  $700^\circ\text{C}$  to  $800^\circ\text{C}$  in increments of  $50^\circ\text{C}$ , and the obtained impedance spectra were processed using ZSimpWin software. For cell performance testing,  $\text{H}_2 + 3\% \text{H}_2\text{O}$ , which can be achieved by bubbling  $\text{H}_2$  through water at about  $25^\circ\text{C}$ , were used as fuel and ambient air as oxidant.

## Results and Discussion

### XRD Analysis

The XRD patterns of  $\text{La}_{0.6}\text{Sr}_{0.4}\text{Co}_{0.4}\text{Fe}_{0.6}\text{O}_3$  powders calcined at different temperatures are shown in Fig. 1a. Although there are some typical diffraction peaks when the calcination temperature is  $900^\circ\text{C}$ , the intensity of diffraction peaks is weak, and there are many impurity peaks. As the calcination temperature increases, several peaks appear at  $2\theta=22.6^\circ, 32.4^\circ, 41.5^\circ, 46.3^\circ$  and  $57.5^\circ$ , which can be attributed to 110, 020, 113, 220 and 024 reflections of the single-phase orthorhombic structure of perovskite  $\text{La}_{0.8}\text{Sr}_{0.2}\text{FeO}_3$ . All the diffraction peak positions are in agreement with those of JCPDF# 35-1480. When the

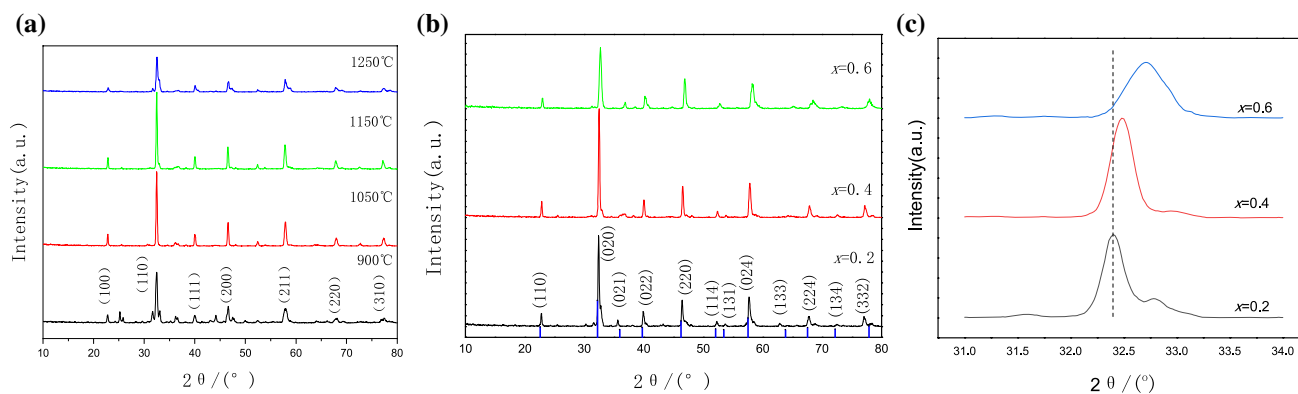


**Fig. 1** XRD patterns of  $\text{La}_{0.6}\text{Sr}_{0.4}\text{Co}_x\text{Fe}_{1-x}\text{O}_3$  cathode powders, (a) samples of  $x=0.4$  calcined at different temperatures, (b) samples with different  $x$  calcined at  $1150^\circ\text{C}$  (blue vertical lines represent the stand-

ard diffraction peak of the  $\text{La}_{0.8}\text{Sr}_{0.2}\text{FeO}_3$ , JCPDF# 35–1480), and (c) magnification of the diffraction peak at  $32.4^\circ$  (Color figure online).

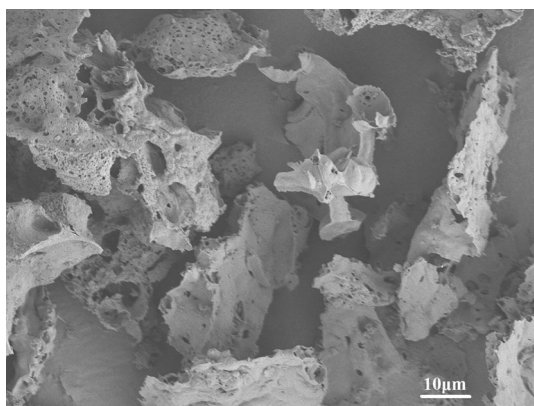


**Fig. 2** SEM photograph of  $\text{La}_{0.6}\text{Sr}_{0.4}\text{Co}_{0.4}\text{Fe}_{0.6}\text{O}_3$  calcined at  $1150^\circ\text{C}$  for 2 h.

calcination temperature reaches  $1050^\circ\text{C}$ , the phase becomes a pure perovskite structure as identified by XRD, indicating that the substitution of  $\text{Sr}^{2+}$  and  $\text{Co}^{3+}$  ions has taken place, and formed a solid solution with the general formula of  $\text{La}_{0.6}\text{Sr}_{0.4}\text{Co}_{0.4}\text{Fe}_{0.6}\text{O}_3$  with a single orthorhombic perovskite phase.

Figure 1b shows the XRD patterns of the LSCF powders with different cobalt dopant content calcined at  $1150^\circ\text{C}$ . All the samples have a single perovskite phase, and there are no obvious impurity peaks. It can be seen from Fig. 1c that with the increase in Co content, the diffraction peak of the corresponding XRD pattern is shifted slightly to higher  $2\theta$  values. This may be due to the incorporation of  $\text{Co}^{3+}$  ions partially replacing the  $\text{Fe}^{3+}$  in  $\text{La}_{0.6}\text{Sr}_{0.4}\text{FeO}_3$ , and resulting in increased lattice distortion. As we know, the radius of  $\text{Co}^{3+}$  and  $\text{Fe}^{3+}$  is 0.061 nm and 0.645 nm, respectively. When  $\text{Fe}^{3+}$  ions were partially substituted by  $\text{Co}^{3+}$ , and with a smaller radius, the lattice constant becomes smaller and the diffraction peaks shift to higher  $2\theta$  values.

## SEM Analysis

The SEM micrograph of the LSCF powder calcined at  $1150^\circ\text{C}$  for 2 h in air is presented in Fig. 2. It can be seen from the figure that the initial powder is a spongy mass with a porous structure. In the process of powder preparation, since all the reactants are uniformly mixed in solution at the atomic or molecular level, reaction can occur through rearrangement and short-distance diffusion of nearby atoms and molecules. During the rapid combustion process, there is not enough energy and time for atoms to diffuse or migrate over long distances, which leads to the growth of nanoscale crystallites. At the same time, due to the high temperature and rapid pyrolysis during the combustion process, a large amount of gas is rapidly released, so that the initial powder forms this fluffy and porous structure.<sup>19</sup> The obtained porous powder helps to achieve the microstructure of the porous electrode.<sup>20</sup>

## Performance of the Single Cell

In order to evaluate the electrode performance, electrochemical impedance spectroscopy (EIS) of YSZ-based cells with the LSCF cathode and Ni/YSZ anode is carried out. Figure 3 shows the Nyquist plots of the single cell tested at different temperatures under  $\text{H}_2$  atmosphere. It can be seen from the figure that the impedance spectrum of the cell consists of two arcs at high frequencies and low frequencies, respectively. The intercept of the impedance arc with the real axis at high frequencies corresponds to the ohmic resistance of the cell. The intercept of the impedance arc with the real axis at low frequencies represents the total resistance of the cell. The distance between the arcs represents the area-specific resistance for the cell. The values of the ohmic and area-specific resistance are summarized in Table I.

It can also be seen from the figure that the arc at low frequencies is much larger than that at high frequencies. As

the temperature increases, the arcs in the impedance spectrum become smaller, which is more obvious for the arc at high frequencies. At low temperatures, oxygen ions cannot

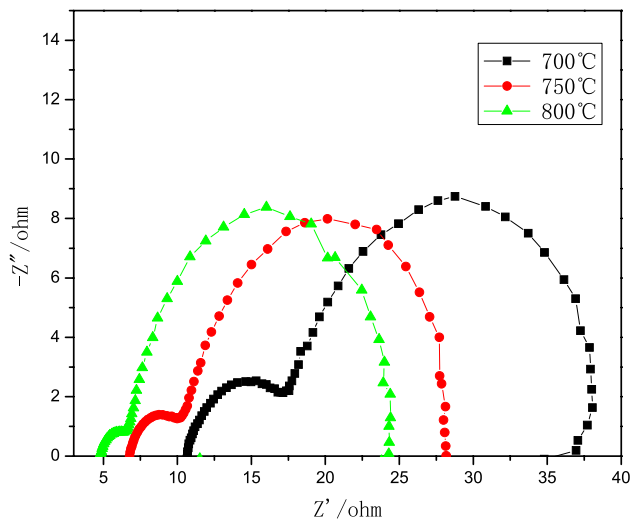


**Fig. 3** Impedance spectroscopy of the single cell.

**Table 1** Electrochemical performance of the  $\text{La}_{0.6}\text{Sr}_{0.4}\text{Co}_x\text{Fe}_{1-x}\text{O}_3$  cathode

	700°C	750°C	800°C
Ohmic resistance ( $\Omega$ )	10.5	6.6	5.0
Area-specific resistance ( $\Omega$ )	26.5	21.6	19.0
Open-circuit voltage (V)	0.98	0.98	1.0
Peak power densities ( $\text{mW}/\text{cm}^2$ )	6	14	28

obtain enough energy from the outside to overcome their transformation barrier, and the charge transfer is controlled by the reaction rate. As the temperature increases, a large number of oxygen ion holes are formed, and capacitance decreases. Therefore, the resistance decreases and the arcs in the impedance spectrum become smaller.

Figure 4 shows the voltage–current ( $V$ – $I$ , Fig. 4a) and power density–current curves (Fig. 4b) of the YSZ-based single cell with LSCF as cathode and Ni/YSZ as anode, using air as oxidant and 3%  $\text{H}_2\text{O} + \text{H}_2$  as fuel. As can be seen from Fig. 4a, the open-circuit voltage of the cell remains almost the same value of 1.0 V at different operating temperatures. Nevertheless, the voltage decreases linearly with the increase in the current, and the lower the operating temperature, the faster the decrease in the voltage. This may be because the voltage is related mainly to the differences in differential pressure of  $\text{H}_2$  and  $\text{O}_2$  across the cell, but has nothing to do with the temperature, so the open-circuit voltage is the same. However, the resistance of the electrolyte decreases as the temperature increases, resulting in a decrease in voltage. In addition, with the increase in the current, the voltage decreases linearly, and the lower the working temperature, the faster the decrease in the voltage.

Figure 4b shows that the power density increases with the increase in current density. When the current reaches a certain value, the power density reaches a maximum, and then decreases. This may be because the power consumed by the internal resistance of the fuel cell increases as the current increases. Once the current reaches a certain value, the output power of the cell reaches the maximum, and then the power consumed by the internal resistance is dominant, which leads to the decrease in the output power of the cell.

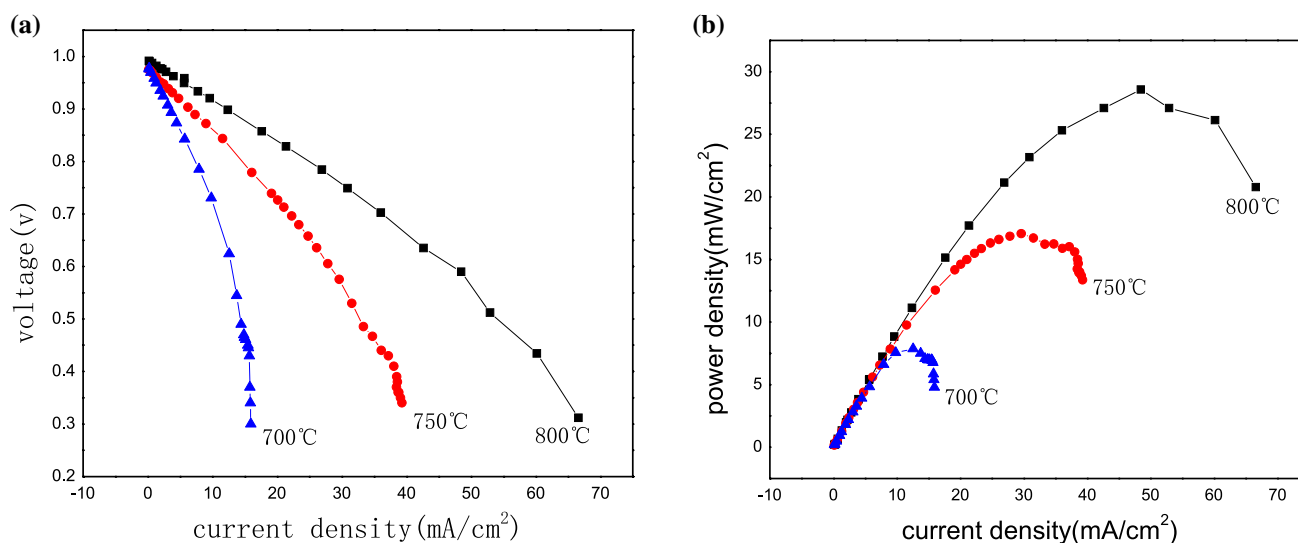


**Fig. 4** The voltage (a) and power density (b) as a function of the current density for the YSZ-based cell with LSCF cathode and Ni/YSZ anode tested from 700°C to 800°C under 3%  $\text{H}_2\text{O} + \text{H}_2$  atmosphere.

The values of open-circuit voltage and peak power densities are also listed in Table I. The peak power density obtained from the single cell performance testing is consistent with the result of the impedance spectrum measurement.

The peak power density is close to that of other cathode materials working in the intermediate temperature range, such as LSCF infiltrated with PNM5,<sup>21</sup>  $\text{Sr}_2\text{Fe}_{1.5}\text{Mo}_{0.5}\text{O}_{6-\delta}$ ,<sup>22</sup>  $\text{Mn}_{1.5}\text{Co}_{1.5}\text{O}_4$ ,<sup>23</sup> and so on. The results show that  $\text{La}_{0.6}\text{Sr}_{0.4}\text{Co}_x\text{Fe}_{1-x}\text{O}_3$  is a promising cathode material for intermediate-temperature SOFC applications.

## Conclusions

In this paper, a series of  $\text{La}_{0.6}\text{Sr}_{0.4}\text{Co}_x\text{Fe}_{1-x}\text{O}_3$  (LSCF,  $x=0.2, 0.4, 0.6$ ) is prepared by citric acid-assisted combustion, and the effect of Co doping on the lattice structure and electrochemical performance of  $\text{La}_{0.8}\text{Sr}_{0.2}\text{FeO}_3$  is systemically investigated. The results of XRD and EIS show that doping with Co induces lattice distortion but does not change its perovskite structure, which improves the electrochemical performance. Among all the samples,  $\text{La}_{0.6}\text{Sr}_{0.4}\text{Co}_{0.4}\text{Fe}_{0.6}\text{O}_3$  demonstrates the best electrochemical performance. The peak power density of the YSZ electrolyte-supported single cell fabricated with the LSCF cathode reaches  $28 \text{ mW cm}^{-2}$  at  $800^\circ\text{C}$ , and it has minimum area resistivity of  $19 \Omega \text{ cm}^2$ . These results suggest that Co doping of  $\text{La}_{0.8}\text{Sr}_{0.2}\text{FeO}_3$  is an effective strategy to improve its electrochemical performance, while  $\text{La}_{0.6}\text{Sr}_{0.4}\text{Co}_{0.4}\text{Fe}_{0.6}\text{O}_3$  is a promising cathode material for intermediate-temperature SOFCs.

**Acknowledgments** This work was supported by the Natural Science Foundation of Anhui Province of China under contact no. 2108085ME152 and the Talent Research Fund Project of Hefei University under contact no. 21-22RC34.

**Conflict of interest** The authors have no competing interests to declare that are relevant to the content of this article.

## References

1. Y. Liu, Z. Shao, M. Toshiyuki, and S. Jiang, Development of Nickel Based Cermet Anode Materials in Solid Oxide Fuel Cells-Now and Future. *Mater. Rep.: Energy* 1, 100003 (2020).
2. M. Beigzadeh, F. Pourfayaz, M. Ghazvini, and M.H. Ahmadi, Energy and Exergy Analyses of Solid Oxide Fuel Cell-Gas Turbine Hybrid Systems Fed by Different Renewable Biofuels: A Comparative Study. *J. Clean. Prod.* 280, 124383 (2021).
3. O. Sharaf and M. Orhan, An Overview of Fuel Cell Technology: Fundamentals and Applications. *Renew. Sust. Energ. Rev.* 32, 810 (2014).
4. K. Al-Hamed and I. Dincer, Development and Optimization of a Novel Solid Oxide Fuel Cell-Engine Powering System for Cleaner Locomotives. *Appl. Therm. Eng.* 183, 116150 (2021).
5. M. Shen and P. Zhang, Progress and Challenges of Cathode Contact Layer for Solid Oxide Fuel Cell. *Int. J. Hydrogen Energ.* 45, 33876 (2020).
6. Z. Lyu, H. Li, Y. Wang, and M. Han, Performance Degradation of Solid Oxide Fuel Cells Analyzed by Evolution of Electrode Processes Under Polarization. *J. Power Sour.* 485, 229237 (2021).
7. B. Maguire, F. Marques, and J. Labrincha, Cathode Materials for Intermediate Temperature SOFCs. *Solid State Ion.* 127, 329 (2000).
8. B. Zhu, Advantages of Intermediate Temperature Solid Oxide Fuel Cells for Tractor Applications. *J. Power Sour.* 93, 82 (2001).
9. Y. Bu, S. Joo, Y. Zhang, Y. Wang, D. Meng, X. Ge, and G. Kim, A Highly Efficient Composite Cathode for Proton-Conducting Solid Oxide Fuel Cells. *J. Power Sour.* 451, 227812 (2020).
10. S. Rehman, R. Song, T. Lim, J. Hong, and S. Lee, Parametric Study on Electrodeposition of a Nanofibrous  $\text{LaCoO}_3$  SOFC Cathode. *Ceram. Int.* 47, 5570 (2021).
11. K. Song, Z. Yu, X. Luo, S. Zhu, Y. Yang, Q. Yang, D. Tian, X. Lu, Y. Ding, Y. Chen, and B. Lin, A Simple Ce-Doping Strategy to Enhance Stability of Hybrid Symmetrical Electrode for Solid Oxide Fuel Cells. *Int. J. Hydrogen Energ.* 45, 29259 (2020).
12. H. Gu, M. Xu, Y. Song, C. Zhou, C. Su, W. Wang, R. Ran, W. Zhou, and Z. Shao,  $\text{SrCo}_{0.8}\text{Ti}_{0.1}\text{Ta}_{0.1}\text{O}_{3-\delta}$  Perovskite: A New Highly Active and Durable Cathode Material for Intermediate-Temperature Solid Oxide Fuel Cells. *Compos. Part B-Eng.* 213, 108726 (2021).
13. A. Abdalla, M. Kamel, S. Hossain, J. Irvine, and A. Azad, Synthesis and Electrochemical Characterization of  $\text{La}_{0.75}\text{Sr}_{0.25}\text{Mn}_{0.5}\text{Cr}_{0.5-x}\text{Al}_x\text{O}_3$  for IT- and HT-SOFCs. *Int. J. Appl. Ceram. Tec.* 17, 1276 (2019).
14. K. Pei, Y. Zhou, K. Xu, Z. He, Y. Chen, W. Zhang, S. Yoo, B. Zhao, W. Yuan, M. Liu, and Y. Chen, Enhanced Cr-Tolerance of an SOFC Cathode by an Efficient Electro-Catalyst Coating. *Nano Energy* 72, 104704 (2020).
15. N. Droushiotis, A. Torabi, M. Othman, T. Etsell, and G. Kelsall, Effects of Lanthanum Strontium Cobalt Ferrite (LSCF) Cathode Properties on Hollow Fibre Micro-Tubular SOFC Performances. *J. Appl. Electrochem.* 42, 517 (2012).
16. G. DiGiuseppe, D. Thompson, C. Gumecci, A. Hussain, and N. Dale, Distribution of Relaxation Times Analysis and Interfacial Effects of LSCF Fired at Different Temperatures. *Int. J. Hydrogen Energ.* 44, 27067 (2019).
17. F. Zhou, Y. Liu, X. Zhao, W. Tang, S. Yang, S. Zhong, and M. Wei, Effects of Cerium Doping on the Performance of LSCF Cathodes for Intermediate Temperature Solid Oxide Fuel Cells. *Int. J. Hydrogen Energ.* 43, 18946 (2018).
18. S. Biswas, T. Nithyanantham, N. Saraswathi, and S. Bandopadhyay, Evaluation of Elastic Properties of Reduced NiO-8YSZ Anode-Supported Bi-Layer SOFC Structures at Elevated Temperatures in Ambient Air and Reducing Environments. *J. Mater. Sci.* 44, 778 (2009).
19. L. da Conceição, A. Silva, N. Ribeiro, and M. Souza, Combustion Synthesis of  $\text{La}_{0.7}\text{Sr}_{0.3}\text{Co}_{0.5}\text{Fe}_{0.5}\text{O}_3$  (LSCF) Porous Materials for Application as Cathode in IT-SOFC. *Mater. Res. Bull.* 46, 308 (2011).
20. Y. Boyjoo, M. Wang, V. Pareek, J. Liu, and M. Jaroniec, Synthesis and Applications of Porous Non-Silica Metal Oxide Submicrospheres. *Chem. Soc. Rev.* 45, 6013 (2016).
21. Y. Shi, Y. Wen, K. Huang, X. Xiong, J. Wang, M. Liu, D. Ding, Y. Chen, and T. Liu, Surface Enhanced Performance of  $\text{La}_{0.6}\text{Sr}_{0.4}\text{Co}_{0.2}\text{Fe}_{0.8}\text{O}_{3-\delta}$  Cathodes by Infiltration Pr-Ni-Mn-O Progress. *J. Alloy. Compd.* 902, 163337 (2022).
22. D. Osinkin, S. Beresnev, and N. Bogdanovicha, Influence of Pr6O11 on Oxygen Electroreduction Kinetics and Electrochemical

- Performance of  $\text{Sr}_2\text{Fe}_{1.5}\text{Mo}_{0.5}\text{O}_{6-\delta}$  Based Cathode. *J. Power Sour.* 392, 41 (2018).
23. Y. Hu, Y. Su, C. Li, C. Li, and G. Yang, Dense  $\text{Mn}_{1.5}\text{Co}_{1.5}\text{O}_4$  Coatings with Excellent Long-Term Stability and Electrical Performance Under the SOFC Cathode Environment. *Appl. Surf. Sci.* 499, 143726 (2020).

**Publisher's Note** Springer Nature remains neutral with regard to jurisdictional claims in published maps and institutional affiliations.